Research article

Study on tank damage and response of adjacent tanks in full time domain of detonation

Yuqi Ding, Baishuai Li, Ye Lu [*], Ming Yang, Jiahe Zhang, Qiaozhen Li, Kai Liu

College of Mechanical Science and Engineering, Northeast Petroleum University Heilongjiang, Daqing 163318, China

A B S T R A C T

The flammable gas volatilized from the storage medium in the tank will burn and explode under the action of an accidental ignition source. Tank explosions formed by the explosive shock wave, explosive debris will not only cause their own damage, but also on the safe operation of adjacent tanks to form a threat. Therefore, in this paper, the vertical dome roof tank is taken as the research object, the criteria of brittle fracture failure of tank materials are constructed, and the multi-field coupling calculation model of tank detonation based on TNT equivalent method is established, taking into account the fluid properties inside and outside the tank, the structure of implosion tank and adjacent tank. By analyzing the full time domain process of gas detonation in tanks under different influence factors, the response to implosion damage of tanks and adjacent tanks under the action of explosion shock wave overpressure and debris was obtained. With the increase of the liquid level, the overpressure and deformation of the shock wave of the detonation tank and adjacent tank decrease, and the type and number of fragments decrease. With the increase of the volume of the tank, the overpressure and stress of the shock wave become larger, the strain rate of the tank becomes larger, and brittle failure is more likely to occur. The types and number of fragments formed increase, but detonation fragments are not formed when the tank is full. The research results in this paper provide a theoretical basis and calculation method for preventing and controlling tank implosion accidents, as well as tank design and tank spacing layout.

1. Introduction

The medium stored in the vertical vault storage tank is combustible, explosive, volatile and easy to generate static electricity, which is easy to cause combustion and explosion accidents under the action of accidental ignition source [1,2]. The shock wave and radiant heat generated by the explosion will cause the tank to self-destruct, and the explosion fragments formed by the explosion may cause a domino effect throughout the tank area, resulting in casualties and heavy property losses in the radiation area. Therefore, it is of great significance to analyze the formation and radiation range of the explosion shock wave, to fully understand the consequences of the explosion of the tank and the reaction of the adjacent tank under the action of explosion to prevent such accidents and reduce the consequences caused by accidents.

The interior of the storage tank is a confined space structure, and the explosion shock wave will produce high frequency super-imposed reflection, which makes the overpressure distribution in

---

The whole structure become very complex. At the same time, the temperature in the space rises sharply and the transient over-pressure phenomenon [3,4]. appears. On the calculation of explosion shock wave in confined space: Geoffrey Chamberlain et al. [5] Statistical analysis of combustible gas explosions caused by leaks from ruptured valves, pumps and pipelines in different regions shows that the release of gases in confined environments can create the right conditions for a strong explosion. Liangyu Cheng et al. [6] carried out the explosion experiment of high-pressure gas pipeline, measured and analyzed overpressure. Ye Lu et al. [7,8] established a combustible gas explosion model inside the small container, simulated the combustible gas explosion process inside the tank structure, and analyzed the heating and overpressure distribution of the inner wall of the tank. S. Høiset et al. [9] A comparison of the results of the blast studies of the Fricksburg accident with the results of the blast simulations shows that the TNT-equivalent method of simulating blast pressures is in general agreement with the estimates in the literature based on calculations rather than visual in-spections. Chongan Pang et al. [10] used the TNT-equivalent model to simulate the implosion of the vertical cylindrical storage tank, and analyzed the enhancement effect of the shock wave overpressure reflection near the tank wall. The tank will be broken under the overpressure of the explosion shock wave, and then forms a missile that has an impact on the adjacent tank. Yunxiong Cai et al. [11] used the experimental method to simulate the hydrocarbon explosion in the vertical dome roof tank, and carried out the correlation analysis of the influence of the hydrocarbon volume fraction, ignition position and liquid level on the explosion shock wave over-pressure. Hamid Rokhy et al. [12,13] Numerical simulations of metal formation by gaseous detonation in stoichiometric mixtures of H_2–O_2 were performed using the CESE-IBM FSI method, comparing the effects of detonation characteristics, midpoint deflection of the workpiece, and initial pressure and temperature of the gas mixture. Good agreement was reached between the numerical results and the empirical data. Hamid Rokhy et al. [14] The CESE-IBM FSI method was used to analyze the explosion characteristics of hydrogen-air mixtures near the concrete barrier and compared with the TNT-equivalent method, which was shown to be more accurate than the TNT-equivalent method. T. Mirzababaie Mostofi et al. [15] The plastic behavior of metal-elastomer bilayers was tested using a mixed gas blast method to increase the impact load threshold. About the question of the consequences of a missile impact: Yang Du et al. [16] A fluid-solid coupling (FSI) simulation of a pipeline fracture due to internal gas detonation is implemented by combining a Lagrangian structure and a Eulerian fluid solver, and dynamic crack extension, strain response, crack velocity, and detonation product expulsion are investigated and discussed. It was found that the method can more reliably predict the fracture mode of a steel pipe subjected to gas detonation loading. Wen hong Wang et al. [17] took the underground closed culvert of the oil and gas leakage as the research object, simulated the explosive fragments of the culvert cover under the influence of certain explosion energy, and quanti-tatively analyzed the flying range of the explosive fragments and the degree of damage caused to the equipment and personnel in the affected area. U. Hauptmanns [18]. Monte Carlo methods were used to analyze the debris flyaway of the pressure vessel explosion to provide a predictive basis for predicting such accidents. Ulrika Nyström et al. [19] Modeled the response of the wall under blast loading, fragmentation loading, and combined blast and fragmentation loading, and the results showed that the overall damage to the wall in the combined loading case was more severe than if the damage caused by blasting and fragmentation loading were added together and treated separately. Rui Feng et al. [20,21] used the Monte Carlo method to study the ejection of the storage tank explosive fragments, and obtained the fragment trajectory curve and the probability distribution of the ejection distance. Siyu Chen et al. [22] established a model of vertical vaulted storage tanks and explosive fragments of different shapes, and used numerical simulation methods to analyze the effect of different fragment shapes and impact velocity on the tank wall. Guohua Chen et al. [23] established a model of pointed fragments produced by the explosion of the vertical vault storage tank, and studied the failure rule of the storage tank under the impact of fragments at different incident angles. Shuai Qi et al. [24,25] used the numerical simulation calculation method to analyze the flying range of explosive fragments in the chemical industry park and the damage degree to equipment and personnel in the affected area. After the calculation method of storage tank explosion shock wave overpressure, explosion fragments, many scholars in how to set the spacing between the tank, the explosion accident rescue reference made the related research: Li Ma et al. [26] The failure of cylindrical containers under impact loads was analyzed to understand the damage mechanism of containers and provide a theoretical basis for the design and life evaluation of explosive containment devices used in engineering. Deming Yu et al. [27] determined the size of the explosion load and the damage area of the tank explosion by numerical simulation, and discussed the damage criteria of the shock wave, put forward the concept of explosion damage/damage partition, and determined the boundary of each area. Xinming Qian et al. [28,29] took the liquid boiling in the ball tank developed into a steam cloud explosion as an example, and used the Monte Carlo method to simulate the ejection range of the fragments and the probability of the target hit by the ejection fragments, so as to judge the safe installation distance of the surrounding storage tanks. Yuqi Ding et al. [30] took the 5000 m [3] vertical vault storage tank as the research object, carried out numerical simulation analysis of the implosion process, and obtained the area affected by explosion radiation under different influencing factors, which provided a theoretical basis for the reasonable layout of tank spacing in the tank area and the rescue of explosion accident.

In conclusion, the existing study separates the response of the explosion tank and the adjacent tank without analyzing the prop-agation process of shock wave overpressure in the explosive tank-air-adjacent tank and the response of the adjacent tank without considering influence factors such as air resistance and gravity. Therefore, the author intends to consider the heterogeneous coupling between tank liquid-tank-air, establish the finite element full-time model of the tank explosive damage process, through the analysis of the tank explosive damage and the reaction of adjacent tank structure, the force of explosive fragments and the flying state, obtain the tank explosive damage and near the tank in the explosion wave overpressure and debris response. The results can provide an important theoretical basis and calculation method for analysis of tank implosion accidents, prevention and control of such industrial disasters, tank design and tank spacing arrangement.

2. Calculation method of tank implosion load and fracture damage of the storage tank

2.1. Analysis of detonation TNT equivalent method of combustible gas in storage tank and implosion destruction form

The combustible gas volatilized from the storage medium in the tank is combustible under the action of an accidental ignition source. As an explosion process, combustion products promote mixed gas work, the spread of the mixed gas speed gradually increases and gradually transforms into the detonation process. Detonation is a rapid release process of combustible gas energy. The TNT equivalent method is usually used to calculate the detonation energy of combustible gas, as shown in Fig. 1.

When the tank volatilizes a certain mass of combustible gas, the shock wave overpressure generated by the combustion and explosion ultimately depends on the equivalent TNT mass of the combustible gas. Therefore, TNT-equivalent method is used to predict the explosion severity, and TNT equivalent is used to represents the power of a vapor cloud explosion.

$$W_{\mathrm{TNT}} = \frac{\beta A W_f Q_f}{Q_{\mathrm{TNT}}} \tag{2.1}$$

Where: W_{TNT} is TNT equivalent of combustible vapor cloud, kg; β is explosive coefficient, usually 1.8 in ground building; A is TNT equivalent coefficient of vapor cloud, value range is 0.02%–14.9% (usually 2.2%); W_f is the total mass of fuel of vapor cloud, kg; Q_f is combustion heat of fuel, kJ/kg; Q_{TNT} is explosive heat of TNT, value range is 4120~4690 kJ/kg (usually 4520 kJ/kg).

As shown in Fig. 1, the tank detonation is accompanied by the destruction of the tank structure, for combustible gas, although the explosion wave overpressure and radiation heat while detonating, but due to the process of explosion propagation speed, short duration, often without transferring the radiating heat to the tank, the tank has already broken, so the impact of the detonation radiation heat for the tank response is small, negligible. At this time, usually under the influence of the overpressure of the rapid explosion shock wave, the storage tank is broken before deformation occurs, the metal material shows obvious brittle fracture and destruction characteristics, and the storage tank breaks and produces fragments; with the occurrence of combustible gas detonation, the fragments fly outward under the continuous action of the explosion shock wave, and the adjacent tank occurs response deformation or failure under the detonation overpressure and fragments impact.

2.2. Node splitting method for brittle fracture and failure of storage tank materials

Due to the fast propagation speed and short duration of shock wave and fragments produced by detonation, the tank structure has been broken before deformation under the action of transient impact load. Therefore, this paper adopts the method of adding bonding units between the nodes of the storage tank material, and analyzes the fracture failure of the tank bonding unit node through the cohesive model. The brittle failure path of the tank bonding unit node is shown in Fig. 2[33].

As can be seen from Fig. 2(a–d), the brittle fracture of the tank material will gradually break and expand along the split direction of the node, for the intermediate node, the split expansion can be opened along multiple paths, while for the corner node, it can only be extended along the unique cell path of the node.

Considering the effective stress strength factor, the fracture standard can be obtained [31,32]:

$$\sigma^{eff} = \sqrt{\sigma + \beta_\tau \tau^2} \geq \sigma_{fr}, \sigma \geq 0 \tag{2.2}$$

$$\sigma^{eff} = \sqrt{\beta_\tau} \left\langle |\tau| - \mu|\sigma| \right\rangle \geq \sigma_{fr}, \sigma < 0 \tag{2.3}$$

Where: β_τ is the shear stress coefficient, μ is the friction coefficient, σ_{fr} is the fracture stress.
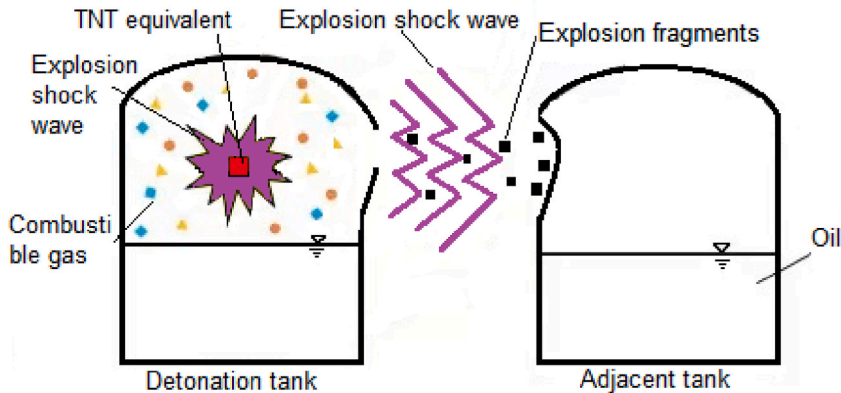

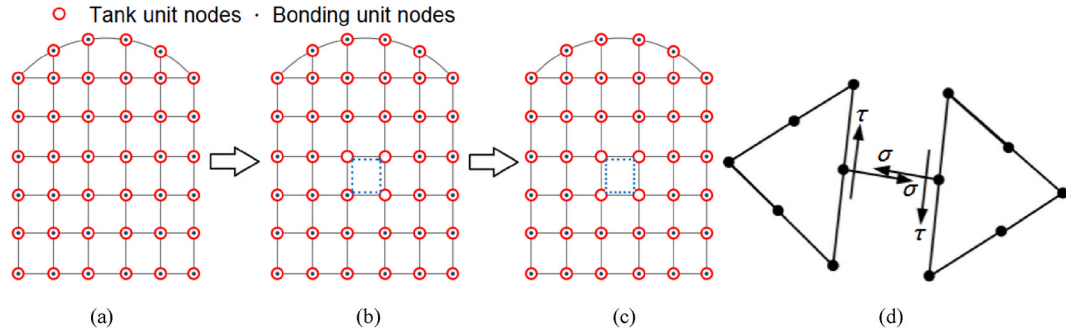**Fig. 1.** Schematic diagram of TNT equivalent method for combustible gas detonation.

Fig. 2. Brittle fracture path of tank bonding element node. (a) Initialize; (b) Crackle; (c) Fragment; (d) Normal stress of fracture node σ and shear stress τ.

The tank material breaks when one of the critical conditions (2.2) or (2.3).

For the implosion load of the material surface of the tank, there is stretching (such as tank top and tank wall) and compression (such as the junction of tank top wall), there are two following conditions, as shown in Fig. 3.

(1) For the stretching of the tank structure unit, as shown in Fig. 3 (a), there are:

$$\sigma = \sigma_0 \left(1 - \frac{\delta_\sigma}{\delta_{\sigma cr}} \right) \tag{2.4}$$

$$\tau = \tau_0 \left(\frac{\delta_\sigma}{\delta_{\sigma cr}} \right) \mathrm{sgn}(\delta_\tau) \tag{2.5}$$

Where: δ_σ and δ_τ are the normal open displacement and sliding displacement respectively; σ_0 and τ_0 are the normal stress and shear stress at the beginning of fracture respectively; $\mathrm{sgn}(x) = x/|x|$ is the sign function.

After a certain opening displacement $|\delta_{\sigma 1}| < \delta_{\sigma cr}$, the crack begins to close, then the traction force follows the linear unloading relationship:

$$\sigma = \sigma_0 \left(1 - \frac{\delta_{\sigma 1}}{\delta_{\sigma cr}} \right) \frac{\delta_\sigma}{\delta_{\sigma 1}} \tag{2.6}$$

$$\tau = \tau_0 \left(1 - \frac{\delta_{\sigma 1}}{\delta_{\sigma cr}} \right) \frac{\delta_\sigma}{\delta_{\sigma 1}} \mathrm{sgn}(\delta_\tau) \tag{2.7}$$
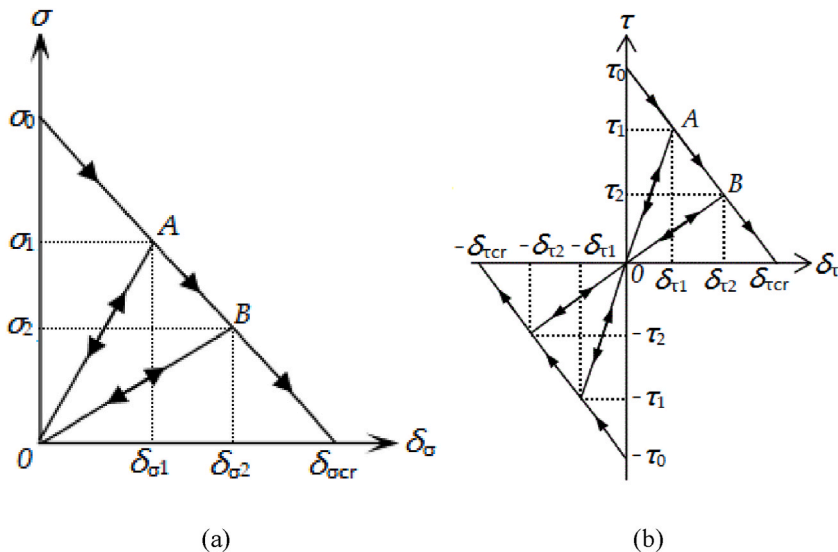

Fig. 3. Change of cohesion of tank material unit. (a) Change in cohesion of tensile element; (b) Change of cohesion of compression unit.

If the crack opens again, the unloading path is reversed to $\delta_{\sigma 1}$, and then follows monotonic cohesion (2.4) and (2.5).

(2) For the tank structure unit being compressed, as shown in Fig. 3 (b):

$$\tau = \tau_0 \left(1 - \frac{|\delta_\tau|}{\delta_{\tau cr}} \right) \text{sgn}(\delta_\tau) \tag{2.8}$$

At the critical sliding displacement $|\delta_\tau| = \delta_{\tau cr}$, the new surface is completely formed and the viscid traction force disappears. If $|\delta_\tau| < \delta_{\tau cr}$, the shear traction follows a linear unloading reloading relationship:

$$\tau = \tau_0 \left(1 - \frac{|\delta_{\tau 1}|}{\delta_{\tau cr}} \right) \frac{\delta_\tau}{|\delta_{\tau 1}|} \tag{2.9}$$

In conclusion, by substituting formula (2.6), (2.7) and (2.9), respectively, into formula (2.2) and (2.3), the tank material bonding unit can be obtained under the action of detonation load node stress. When the tip of the specified distance before the interface local stress reaches the critical value, the crack tip node will be separated, the tank material fracture.

3. Establishment of the storage tank detonation finite element model considering the internal and external fluid domain

3.1. Analysis of the force state of the combustible gas detonation in the storage tank

During the detonation process of the combustible gas in the tank, the tank body is mainly affected by the impact pressure of the explosion. Therefore, in order to facilitate the analysis of the full time domain process of the detonation of the storage tank, according to the variation between the pressure generated and the action time during detonation, the interaction process of the detonation of combustible gas and the storage tank in the tank is divided into four stages. The load changes of the detonation tanks and adjacent storage tanks in different stages are shown in Fig. 4.

As can be seen from Fig. 4, at the beginning of the first detonation stage: the combustible gas in the tank is ignited, at this time, the storage tank is only affected by its own gravity G and hydrostatic pressure Poil of the liquid in the tank; at the end of the first stage: when the pressure generated from the gas detonation in the tank spreads to the tank, except its own gravity and hydrostatic pressure, also affected by the pressure load $P(t)$ produced by the detonation; at the end of the second stage: due to the brittle failure of the tank material under the high pressure caused by detonation, resulting in the tank cracking and pressure leakage, so the load $P(t)$ on the tank surface changes; at the end of third stage: under the continuous high pressure of the detonation load, the storage tank produces different explosion fragments of different sizes and different speeds; at the end of the fourth stage: the fragments flies under the continuous detonation load and reaches the adjacent storage tank, while the adjacent storage tank is deformed and even broken under the action of the detonation load $P(t)$ and the fragments hitting $V(t)$.

3.2. Establishment of 3D finite element model in the full time domain of storage tank detonation

In this paper, the vertical dome roof tank is taken as the research object, the storage tank structure is composed of the dome, the tank wall and the tank bottom plate. Considering the force characteristics of the tank structure and the detonation process, the tank structure of the breather valve and the weld is ignored, and the tank structure is equivalent to the spherical shell and the cylindrical shell structure. In this paper, 1000 m [3] and 3000 m [3] are taken as examples, where 1000 m [3] tank is equal wall thickness structure, the inner diameter D is 10800 mm, the tank height H is 13661 mm, 3000 m [3] tank is variable wall thickness structure, the inner diameter D is 15000 mm, the tank height H is 19460 mm, the tank materials are Q235B, the material parameters are shown in Table 1.

The distance between the detonation tank and the adjacent tank is set to 0.75D (0.6D) according to the standard [33]. In order to describe the complete propagation process of the explosion shock wave, considering the model size and calculation stability, after several tests, it was determined that the external air domain of the tank extends 1.6 m outward and 2.34 m upward, and the air domain
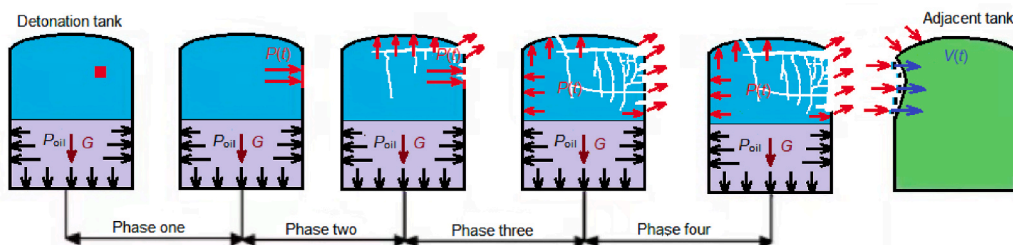

Fig. 4. Schematic diagram of load transfer in tank during combustible gas detonation.

Table 1
Q235 performance parameters of storage tank material.

Temperature/ °C	Young's modulus/ 1011Pa	Poisson's ratio	Yield strength /MPa	Specific heat capacity /MPa	Cohesive strength of bonding element /MPa	Rigidity /(N/ mm^3)	Fracture energy /(kJ/m^2)
22	2.02	0.3	235	461	517	106	847

Note: The material performance parameters of the storage tank change with the change of temperature. Based on the space limit, this paper only lists the parameters at 22 °C.

is length (1.6 × 2 + 0.75D(0.6D) + 2D) m, width (0.5D + 1.6) m, and height (H + 2.34) m. According to the tank geometry, the three-dimensional finite element model of tank fluid domain is established as shown in Fig. 5(a and b), where the air domain and tank liquid are solid unit, the tank adopts shell unit, the model is half modeling to reduce the calculation amount, the tank is described by Lagrange grid, TNT explosive and fluid are described by Euler grid. In the process of the full time domain of detonation in the tank, the tank gas transfers the shock wave overpressure to the tank domain, at this time, the maximum bonding unit node stress σ^{eff} at the tank wall is greater than the fracture stress σ_{fr} (517 MPa), the bonding unit nodes separate to form explosion fragments; then shock wave overpressure, radiant heat and explosion fragments are transmitted to the air domain and eventually to the adjacent tank, and affects the adjacent storage tank. Load is transferred between the domains through contact, and symmetrical boundary conditions are applied to the symmetrical surface to describe the overall force of the tank. In terms of size setting of the tank and air domain grid, the tank structure unit divides the grid according to the principle of unit proportion limit and monitors the maximum stress point; the tank unit divides the grid and monitors the maximum pressure point of fluid; when the maximum pressure value of the tank are stable within the 5% variation range, then the unit size of the numerical model is determined. Ensure the node corresponding condition of the tank wall and the fluid wall inside the tank, after calculation, the size of 1000 m [3] tank and air domain cell grid is 0.125 m, and the size of 3000 m [3] tank and air domain cell grid is 0.175 m.

In order to describe the explosion shock wave overpressure, tank deformation and fragments response from the detonation tank close to and away from the explosion center and adjacent tank wall, the monitoring point as shown in Fig. 5(a) is set, where the "1″" series points are the monitoring points near the explosion center, the "1' " series points are the far away from explosion center monitoring points, the "2″" series points are the adjacent tank monitoring points; point O corresponds to the initiation center, point T corresponds to the tank top, point E corresponds to the top wall junction, point C corresponds to the flush position of the explosion center, point B corresponds to the flush position of the liquid level, point A corresponds to the bottom wall junction.

4. Tank fracture and response of adjacent tank during the detonation full time domain

4.1. Analysis of tank structure under detonation load

In this paper, taking the 1000 m [3] tank eccentric explosion (2.7,0,9.125) and half tank (liquid level height 7.08 m) as examples, the mixture of methane and air as combustible gas in the tank, the liquid in the tank is crude, and the concentration of volatile methane in the tank is the explosive concentration of 9.5% (TNT equivalent is about 22 kg). In order to analyze the flow field of the tank structure under the action of detonation load, the pressure distribution in the tank when the explosion pressure spreads to the tank wall (1.4 ms) and the cracking time (3.2 ms) is shown in Fig. 6, the pressure change curve over time at the left and right sides of the
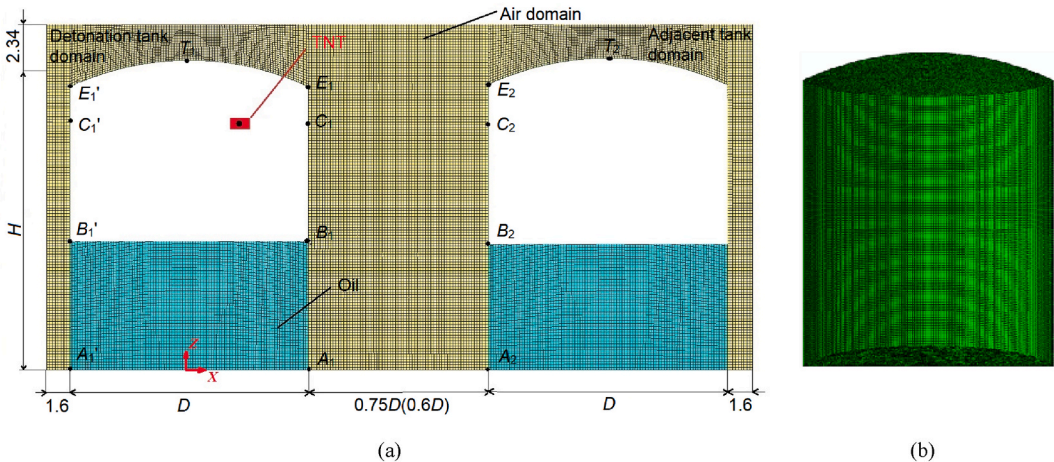

(a) (b)

Fig. 5. Full time domain finite element model of combustible gas detonation in tank. (a) Flow field model of implosion; (b) Finite element model of tank structure.
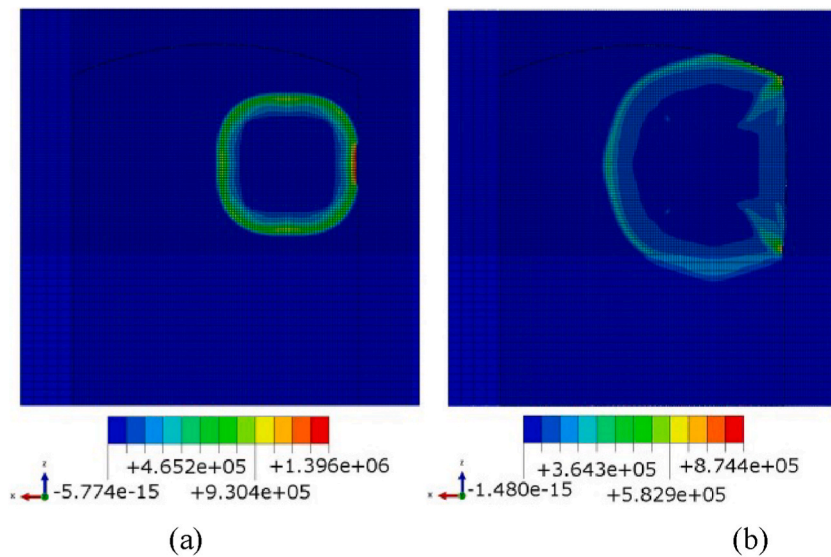
Fig. 6. Cloud chart of detonation tank pressure distribution at point different.

monitoring points of the explosion center is shown in Fig. 7, and the peak pressure and the time data at different monitoring positions are shown in Table 2.

As can be seen from Fig. 6(a and b), the detonation shock wave spreads outward in the form of spherical wave at the Initiation position. At 1.4 ms, the detonation shock wave reaches the tank wall, the overpressure near the tank wall will increase due to the wall reflection and wave convergence effect; at 3.2 ms, the storage tank begins to produce cracks, and the detonation pressure spreads outward from the crack, and the pressure is further reduced. As can be seen from the data in Fig. 7 and Table 2, the pressure of each monitoring point gradually increases with the propagation of the explosion shock wave, and begins to decrease after reaching the peak. Whether close to the explosion center or away from the tank wall of the explosion center, point C_1 (C_1') directly opposite the explosion center first showed peak pressure at 1.6 (18.2) ms; although the height of the liquid level (B_1) and the top wall junction (E_1) are the same distance from the explosion center, however, the reflection enhancement effect at the top wall junction (E_1), therefore, the peak pressure (1160.2 kPa) at point E_1 is 70.0% greater than that at point B_1 (682.4 kPa); the peak pressure at E_1 is 63.4% smaller than at C_1 (3170.3 kPa), while the peak pressure (846.2 kPa) at E_1' is 196.8% greater than at C_1' (285.5 kPa), this is because the tank wall near the explosion center causes the detonation pressure to spread outward, and far away from the explosion center without a crack, E_1' due to the reflection enhancement effect, the peak pressure has exceeded the C_1' point directly opposite the explosion center, this indicates that the reflection enhancement effect at the top wall junction cannot be underestimated.

4.2. Analysis of fracture and failure of storage tank structure under detonation load

4.2.1. Structural stress and deformation analysis of detonation of combustible gas in storage tank

In order to further analyze the structural stress and deformation of the tank caused by detonation, the stress distribution of the tank
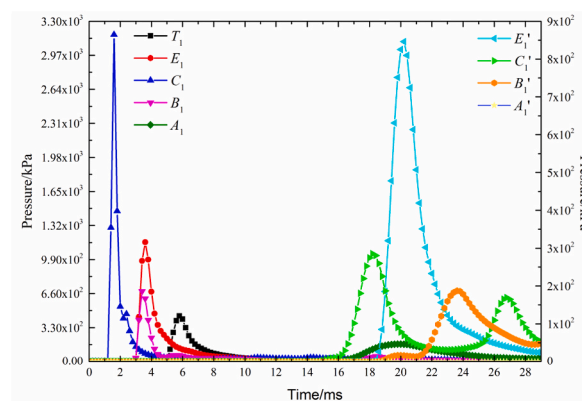

Fig. 7. Pressure change curve of each monitoring times.

Table 2
Comparison of peak pressure and time data at different monitoring points.

Monitoring site	Peak time/ms	Pressure/kPa	Monitoring site	Peak time/ms	Pressure/kPa
T_1	5.8	444.3	–	–	–
E_1	3.6	1160.2	E_1'	20.2	846.2
C_1	1.6	3170.3	C_1'	18.2	285.5
B_1	3.4	682.4	B_1'	23.6	18.5
A_1	20	170.1	A_1'	29	0

at the time of initial crack (3.2 ms), fragmentation (5.2 ms) and fragmentation no longer increasing (29 ms) were extracted respectively, as shown in Fig. 8. The pairs of stress displacement data at different monitoring points are shown in Table 3.

It can be seen from the data in Fig. 8(a and b) and Table 3 that the maximum stress at the tank wall is 252.9 MPa at 3.2 ms, which is greater than the yield strength of the material (235 MPa). At this time, the maximum bonding unit node stress of the tank σ^{eff} is greater than the fracture stress σ_{fr} (517 MPa), the bonding unit node is separated, and the tank begins to crack. At 5.2 ms, the four nodes of the bonding unit at the crack tip were separated, and the material of the tank was fractured and fragmented. At this time, the maximum stress at the tank wall was 435.2 MPa. At 29 ms, the fragments does not increase and the maximum stress is 638.8 MPa. Although the pressure in the tank at the point C_1 directly opposite the detonation center is the maximum at the initial moment, the stress value is very small because it is not applied to the tank. Therefore, at the moment 3.2 ms, the stress at the point E_1 at the top wall junction (159 MPa) is the maximum value of each monitoring point, which is 28.9% larger than the stress at point C_1 (113 MPa). With the process of detonation, the detonation pressure continued to decrease, and the pressure was slightly increased by reflection enhancement after passing to the tank wall, and the stress value greatly increased by the effect of detonation pressure. At 5.2 ms, the stress at point C_1 (178 MPa) exceeded that at point E_1 (129 MPa), which was 27.5% larger than point E_1. Because detonation is a typical brittle failure and the strain rate is very high, the brittle failure occurs before the tank has time to produce large deformation. Therefore, at the moment of 3.2 ms, the stress directly opposite the detonation center point C_1 is very large, but the deformation is only 60.9 mm. At 5.2 ms, the deformation at the point directly opposite the explosion center point C_1 reached 137.1 mm due to the fragmentation caused by the crack diffusion of the tank.

4.2.2. Velocity analysis of tank fragments

In order to further analyze the velocity of the tank, there are 12 fragments of 7 different shapes with the largest energy and speed near the adjacent tank were extracted at no increase (29 ms). The distribution of fragments is shown in Fig. 8(c). The average velocity distribution of the fragments of each shape is shown in Fig. 9, and the quality and average velocity of all kinds of fragments are shown in Table 4.

As can be seen from Fig. 9 and Table 4, since the class *c* fragment is close to the initiation center and the fragment mass is relatively small, the average velocity of class *c* explosive fragments is maximum, reaching 46.3 m/s; although the class *a* fragment is closest to the initiation center, due to the maximum mass of the class *a* fragments, the velocity of the class *a* fragment is smaller than the class *c* fragment; class *g* fragments, although farther from the initiation center than fragments *a*, *c*, are the second fastest of all fragments due to their smallest mass; the other fragments are far away from the initiation center and have low detonation pressure, so the speed is smaller.

4.3. Study on the radiation effects of tank detonation on adjacent tanks

4.3.1. Flow field analysis of adjacent tank structure under detonation load

As the detonation process progresses, the detonation shock wave pressure spreads outward from the rupture of the detonation tank and finally reaches the adjacent tank. The cloud map of the detonation pressure distribution at the time when the shock wave pressure
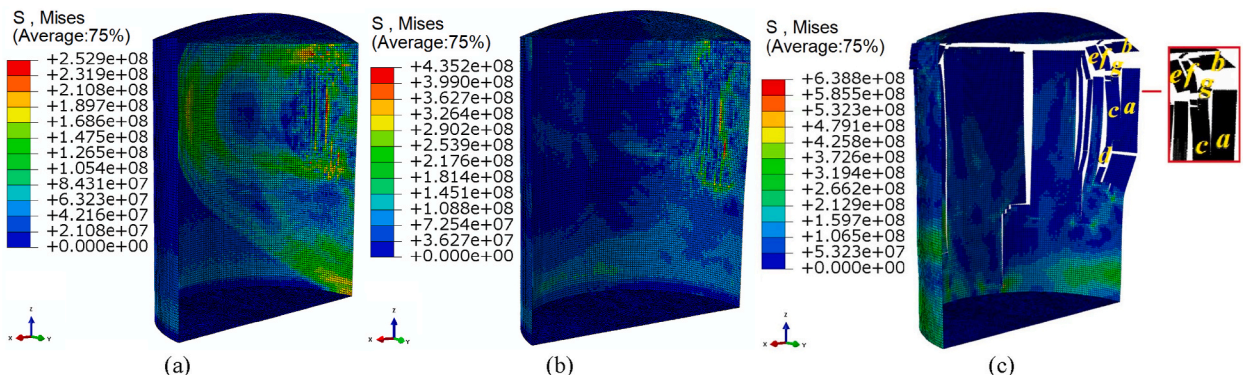

Fig. 8. Equivalent stress distribution diagram of storage tank at different times(Pa). (a)3.2 ms; (b)5.2 ms; (c)29 ms.

Table 3

Comparison of stress and displacement data at different monitoring points.

| Monitoring point	Time /ms	Stress /MPa	Difference from the maximum	Deformation /mm	Time /ms	Stress /MPa	Difference from the maximum	Deformation /mm
T_1	3.2	10	−93.7%	0	5.2	36	−79.8%	0.3
E_1	3.2	159	Maximum	2.1	5.2	129	−27.5%	30.4
C_1	3.2	113	−28.9%	60.9	5.2	178	Maximum	137.1
B_1	3.2	102	−35.8%	3.6	5.2	85	−52.2%	19.6
A_1	3.2	46	−71.0%	0	5.2	46	−74.2%	0
E_1'	3.2	5	−96.8%	0.4	5.2	70	−60.6%	1.6
C_1'	3.2	2	−98.7%	0.3	5.2	18	−89.9%	1.4
B_1'	3.2	2	−98.7%	0.3	5.2	76	−57.3%	0.9
A_1'	3.2	46	−71.0%	0	5.2	46	−74.2%	0
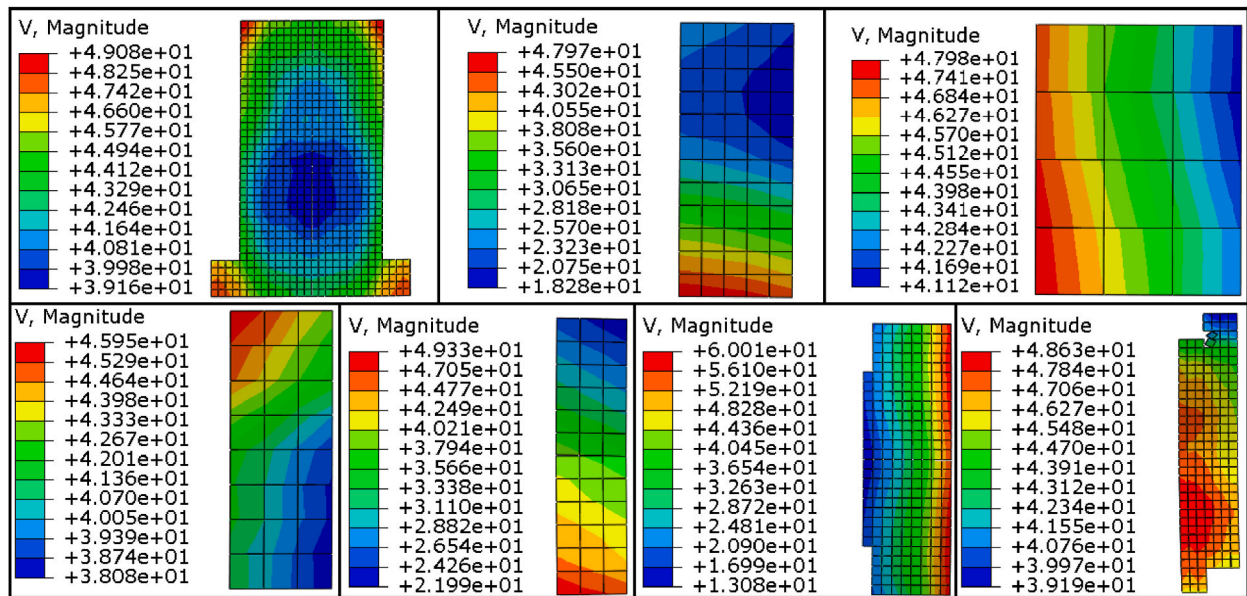
Fig. 9. Initial velocity distribution of various fragments in the tank at 29 ms (Pa).

Table 4

Statistical table of average velocity quality of various fragments in storage tank.

Fragment type number	a	b	c	d	e	f	g
Quantity	1	1	2	2	2	2	2
Quality/kg	437.5	132.3	115.9	13.1	32.8	19.7	6.6
Average velocity/(m/s)	42.7	35.1	46.3	41.4	28.4	36.2	44.7

reaches the adjacent tank (65 ms), and the pressure over time change curve of the monitoring points of the near storage tank are shown in Figs. 10 and 11, and the peak pressure data of different monitoring points of the near storage tank are shown in Table 5.

It can be seen from Fig. 10(a and b), the explosion shock wave overpressure in 65 ms time to near the storage tank, shock wave overpressure mainly concentrated in the top wall junction (E_2), on the explosion center (C_2) and level height (B_2), This is because the explosion position of the detonation storage tank occurs in the area of the three monitoring points, as a result, the shock wave overpressure distribution near the storage tanks is mainly concentrated at the corresponding monitoring points. As can be seen from the data in Fig. 11 and Table 5, The time change curve of the adjacent tank monitoring point pressure fluctuates after reaching the peak pressure, Point C_2 is due to the destruction of the tank at the corresponding location, so the pressure drops to 0; top wall junction (E_2) is 17.0 kPa at 70 ms, After that, it presents a fluctuating state with time change; the peak pressure at the explosion center (point C_2) is 16.1 kPa at 90 ms time; at the A_2 and T_2 monitoring points far away from the break position of the detonation storage tank, the time to reach the peak pressure was 175 ms and 185 ms, respectively, the peak pressure is calculated at 14.2 kPa and 12.2 kPa.

4.3.2. Fracture analysis of adjacent tank structure under detonation load

Since the adjacent tank is simultaneously affected by the explosion shock wave pressure and the explosion fragments, in order to
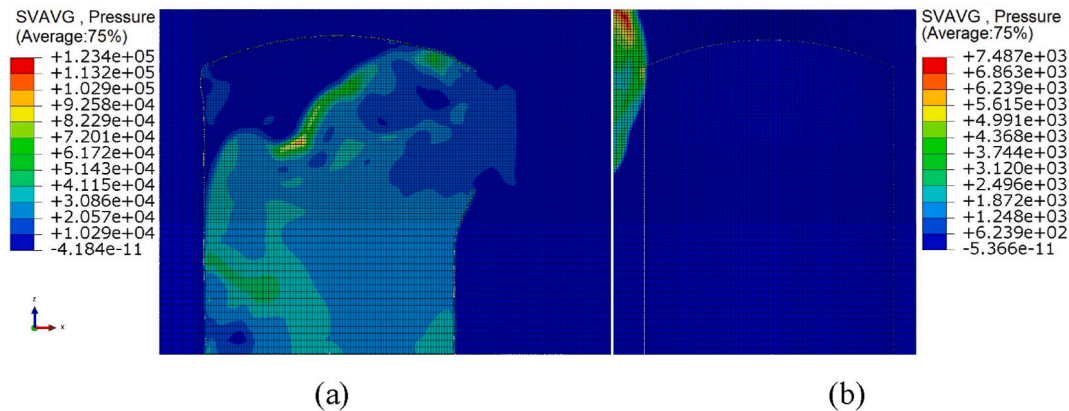
Fig. 10. Cloud chart of detonation pressure distribution inside and outside the tank at 65 ms (Pa).

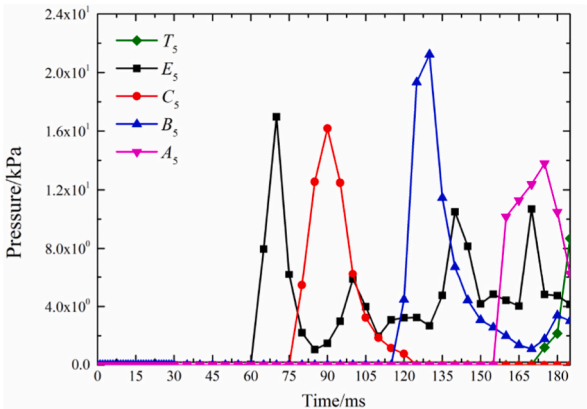**Fig. 11.** Pressure change curve of each monitoring point with time.

Table 5

Pressure data sheet of different monitoring points near the storage tank.

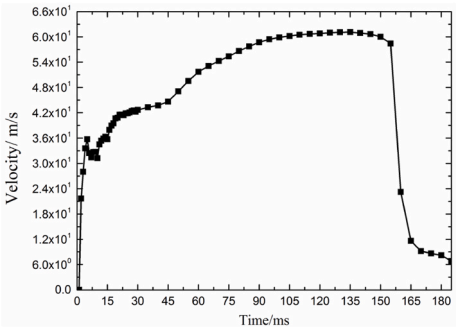| Monitoring point	A_2	B_2	C_2	E_2	T_2
First peak time/ms	175	130	90	70	185
Pressure/kPa	14.2	21.1	16.1	17.0	12.2

Fig. 12. Time varying curve of maximum energy fragment average velocity.

illustrate the stress and deformation changes of the adjacent tank, the average velocity curve of the maximum energy fragments over time is extracted respectively, as shown in Fig. 12. The stress distribution of the tank when the explosion fragments spreads to the adjacent tank (155 ms) is shown in Fig. 13. The stress curve of each monitoring point over time is shown in Fig. 14, and the stress, deformation and fragments velocity data of each point at different times are shown in Table 6.

As can be seen from Fig. 12, after detonation, the velocity of the tank rises rapidly, reaching the first peak of 36.3 m/s within 4 ms. Subsequently, the velocity decreased to 32.4 m/s due to the breakage and fragmentation of tank materials at 5.2 ms, and reached the maximum peak at 61.1 m/s at 135 ms. Then, under the action of the air resistance outside the tank, the velocity of the fragments dropped to 58.4 m/s, when it flew near the adjacent tank, and decreased to 6.8 m/s when the fragments hit the adjacent tank at 155 ms. As can be seen from Fig. 13, at 155 ms, fragments of the detonation tank flew into the adjacent tank, the stress value at the site impacted by fragments increased rapidly, and the tank began to crack, with the stress near the break reaching 271 MPa. As can be seen from Fig. 14 and Table 6, with the process of the detonation, due to the continuous fluctuation of the pressure near the storage tank, the stress of the monitoring points near the storage tank fluctuates; at 155 ms, the stress value directly opposite the explosion center (point C_2) was reduced to 0 due to the fragments shock on the adjacent tank. The peak stress of 168 MPa and 243 MPa was reached at 185 ms and 160 ms respectively at the liquid level near the breach (B_2 point) and the top wall joint (E_2 point) after being hit by fragments. Based on the analysis of the stress and tank damage at the monitoring points near the tank, the fragments flight has caused the tank to break, and the tank has completely lost its working ability.

5. Analysis of storage tank implosion and accident prevention under different influencing factors

5.1. Analysis of tank fracture and adjacent tank under different detonation conditions

5.1.1. Analysis of storage tank fracture and damage under different detonation conditions

In order to analyze the influence of storage level and tank volume size on the fracture damage of storage tanks, analyze the response of the implosion structure of storage tank under 1000 m [3] vault tank at eccentric explosion (2.7,0,6.5), empty tank (height 0.5 m) and full tank (level 10.37 m); 3000 m [3] vault tank at eccentric explosion (3.75,0,9.15), empty tank (0.5 m) half tank (9.98 m) and full tank (level 14.72 m). After calculation, the stress distribution of the tank at the time of termination under different detonation conditions is calculated as shown in Fig. 15; to further analyze the influence of the pressure and the maximum stress position of the different detonation conditions extract the data on the explosion center (C_1) and the top wall junction (E_1), for the deformation of the tank pressure stress and the number of fragment types at the moment of fragment generation and no longer as shown in Table 7.

As can be seen from the data in Fig. 15(a–c) and Table 7, as the elevated fluid level, less combustible gas equivalent within the tank, the shock wave overpressure becomes smaller, lead to less stress and deformation, reduced species and number of fragments produced, no fragments is produced under the full tank condition; however, due to the maximum combustible gas equivalent and large detonation energy, the tank starts to produce fragments before its peak pressure, fast pressure relief speed, therefore, the shock wave overpressure of the empty tank is less than half the tank, the stress and deformation of the empty tank is also less than half of the tank; since the starting position of the empty tank is far from the top wall junction (E_1), and the tank first appears broken at the opposite center (C_1), leading the stress (141.3 MPa) at the 1000 m [3] empty tank level is 9.5% larger than the half tank level (129.0 MPa). As the storage tank volume becomes larger, greater gas TNT equivalent in the tank, leading to a larger shock wave overpressure, and lead to increased stress, but the deformation is smaller; this is because as the tank volume increases, increased combustible gas in the tank, leading to an increased detonation load, the storage tank strain rate becomes larger and more vulnerable to brittle damage; since the 3000 m [3] tank occurs after detonation, the tank broke immediately at the explosion center, the detonation pressure in the tank is rapidly leaked out, therefore, the stress (78.4 MPa) of the 3000 m [3] half tank at the explosion center (C_1 point) is 56.1% smaller than that of the 1000 m [3] half tank (178.1 MPa).
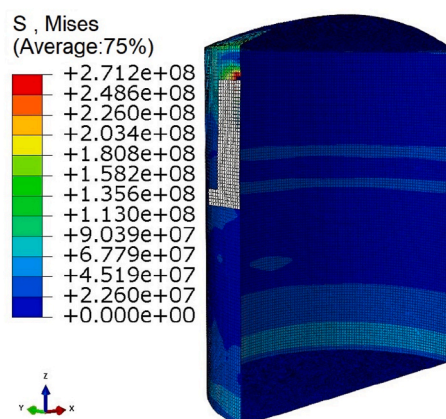

Fig. 13. Cloud chart of stress distribution of 155 ms adjacent storage tank.
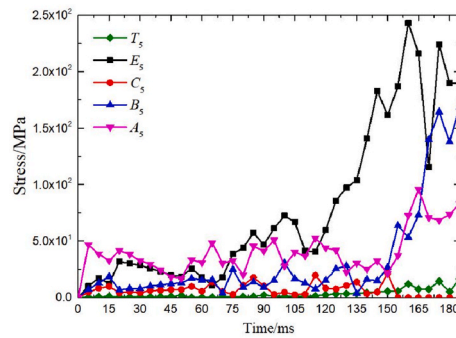
Fig. 14. Time varying curve of stress at each monitoring point.

Table 6
Data sheet of stress, deformation and fragment velocity at different times at each monitoring point.

Time /ms	Stress/MPa					Deformation					Fragments velocity/ m/s
	T_2	E_2	C_2	B_2	A_2	T_2	E_2	C_2	B_2	A_2	
155	6	161	Crevasse	27	21	2.7	2.1	Crevasse	5.2	0	58.4
185	17	189	Crevasse	168	83	8.4	12.9	Crevasse	66.4	0	6.8
Peak time (ms)	17 (185)	243 (160)	21 (150)	168 (185)	96 (165)	8.4 (185)	12.9 (185)	6.3 (150)	67.4 (185)	0	61.1 (135)

(a)   (b)   (c)
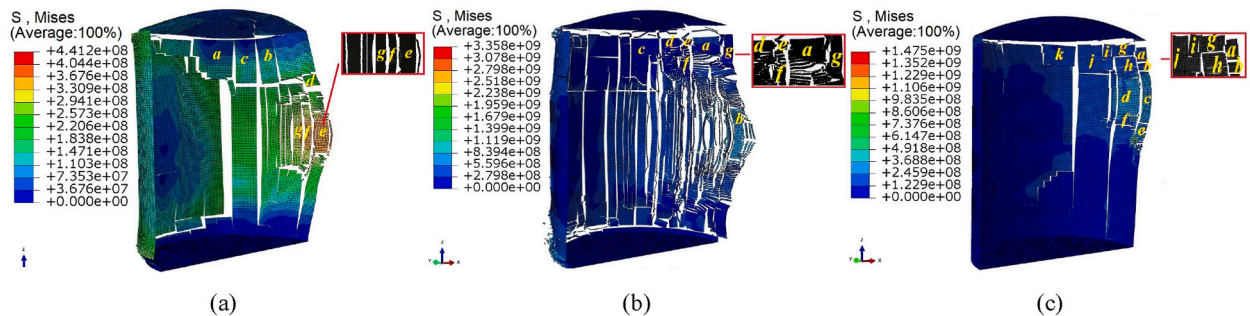
Fig. 15. Stress distribution diagram of storage tank at the end of calculation under different detonation conditions (Pa).(a) 1000 m [3] Empty tank at 32 ms; (b) 3000 m [3] Empty tank at 42 ms; (c) 3000 m [3] Half tank at 30 ms

5.1.2. Response analysis of adjacent storage tanks under different detonation conditions

In order to analyze the response situation of the adjacent tank under different detonation conditions the stress distribution of the adjacent tank under different volume and liquid level is extracted as shown in Fig. 16 The data on the detonation pressure at the explosion center (C_2) and the top wall junction (E_2) are calculated as shown in Table 8.

According to the data in Fig. 16(a–c) and Table 8, since the explosion height of 3000 m [3] is lower than that of half tank (13.1 m), the corresponding position of the damage of the adjacent tank is lower, the 3000 m [3] tank TNT equivalent is larger, the size of the explosion of the adjacent tank is larger, and the shock wave overpressure is smaller, so the influence on the adjacent tank is smaller. For different levels near the tank, similar to the detonation tank, is the center (C_2) and the top wall junction (E_2) pressure, stress and deformation are reduced with the increase of the level, but due to the empty tank level of detonation tank pressure, stress and deformation is less than half a tank, so near the tank peak pressure, stress and deformation is maximum, empty tank second, full tank is minimum. In terms of the different volumes, as the storage tank volume increases, increasing peak pressure and stress at the positive center (C_2) and the top wall junction (E_2), the time to reach the peak pressure decreases; this is because, after the storage tank volume increases, the shock wave overpressure formed in the detonation storage tank increases, early peak arrival time near the tank, the peak time value becomes larger; and for the full tank, since the 3000 m [3] tank formed broken under the detonation load, while the 1000 m [3] tank formed a crack, causes the different overpressure propagation path of the detonation shock wave, the peak arrival time of full tank pressure is slower than that of 1000 m [3], the values do not change much.

Table 7

Comparison table of pressure, stress, deformation and number of fragments at C_1 and E_1 monitoring points.

| Volume /m³	Moment	Liquid level	Time /ms	C_1 Pressure /kPa	Stress/ MPa	Deformation/ mm	E_1 Pressure /kPa	Stress/ MPa	Deformation/ mm	Liquid level	TNT Equivalent /kg	Fragment types	Fragment number
1000	Start to produce fragments moment	Empty	3.8	9.1	53.7	14.9	0.2	141.3	14.1	Empty	37.9	17	34
		Half	5.2	34.7	178.1	137.1	191.9	129.0	30.4				
	Relative difference		26.9%	73.7%	69.8%	89.1%	99.9%	−9.5%	53.6%	Half	22.0	11	19
	No more fragments moment	Empty	32	Crevasse	Crevasse	Crevasse	43.9	19.3	332.1				
		Half	29	Crevasse	Crevasse	Crevasse	Crevasse	Crevasse	Crevasse	Full	4.2	0	0
		Full	34	Crack	Crack	Crack	23.6	71.9	10.2				
3000	Start to produce fragments moment	Empty	4.2	22.2	69.1	7.3	43.1	137.9	0.4	Empty	105.7	39	75
		Half	5.6	48.2	78.4	107.0	40.7	145.5	29.4				
	Relative difference		25%	53.9%	11.8%	93.1%	−5.8%	5.2%	98.6%	Half	59.0	15	26
	No more fragments moment	Empty	42	Crevasse	Crevasse	Crevasse	Crevasse	Crevasse	Crevasse				
		Half	30	Crevasse	Crevasse	Crevasse	Crevasse	Crevasse	Crevasse	Full	9.3	0	0
		Full	36	Crevasse	Crevasse	Crevasse	Crevasse	Crevasse	Crevasse				
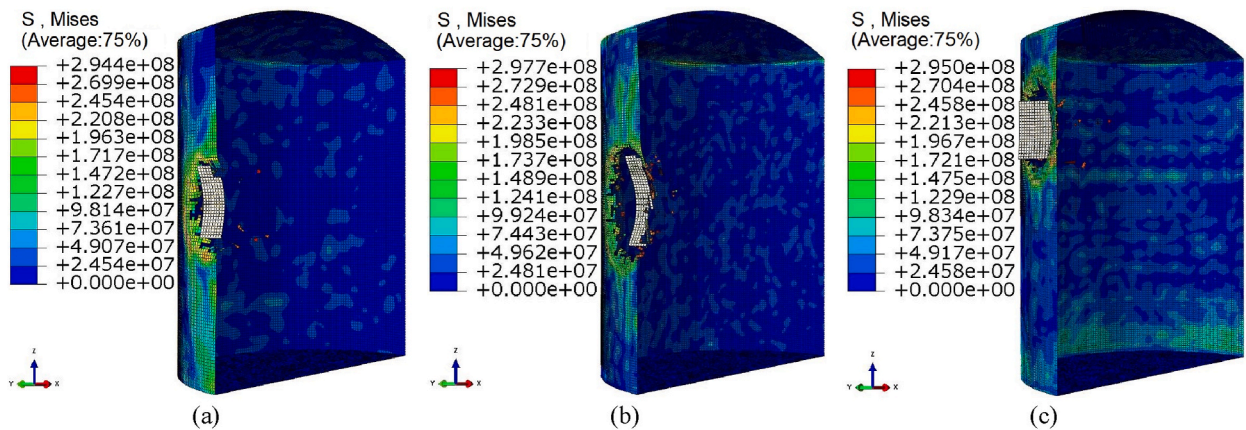
Fig. 16. Stress distribution diagram of adjacent storage tank under different volume and liquid level conditions (Pa). (a)1000 m [3] Empty tank; (b) 3000 m [3] Empty tank; (c)3000 m [3] Half tank.

Table 8
Comparison table of pressure stress and deformation data of C_2 and E_2 monitoring points at different times.

Volume /m³	Liquid level (TNT equivalent)	C_2				E_2			
		Time /ms	Pressure /kPa	Stress /MPa	Deformation/ mm	Time /ms	Pressure /kPa	Stress /MPa	Deformation/ mm
1000	Empty (37.9 kg)	58	6.1	2	0.7	88	11.6	1	0.1
		Peak moment	6.5 (63 ms)	6 (98 ms)	0.8 (103 ms)	Peak moment	12.4 (93 ms)	150 (129 ms)	3.3 (138 ms)
		158	Crevasse	Crevasse	Crevasse	138	9.8	23	3.3
	Half (22.0 kg)	65	14.6	6	0.5	65	16.6	1	0.5
		Peak moment	15.0 (60 ms)	21 (150 ms)	6.3 (150 ms)	Peak moment	17.0 (70 ms)	243 (160 ms)	12.9 (185 ms)
		185	Crevasse	Crevasse	Crevasse	185	9.6	189	12.9
	Full (4.2 kg)	210	0.8	19	2.0	205	1.3	16	1.4
		Peak moment	1.0 (221 ms)	17 (225 ms)	0.6 (225 ms)	Peak moment	1.5 (225 ms)	34 (225 ms)	1.9 (225 ms)
		225	0.9	17	0.6	225	1.5	34	1.9
3000	Empty (105.7 kg)	33	14.5	2	0.5	73	16.0	222	1.1
		Peak moment	14.5 (33 ms)	46 (93 ms)	19.4 (78 ms)	Peak moment	16.3 (78 ms)	222 (73 ms)	7.2 (143 ms)
		152	Crevasse	Crevasse	Crevasse	152	13.6	105	6.1
	Half (59.0 kg)	51	19.8	18	1.7	61	18.1	7	0.6
		Peak moment	20.6 (56 ms)	80 (141 ms)	27.2 (146 ms)	Peak moment	18.6 (66 ms)	245 (160 ms)	13.7 (181 ms)
		206	Crevasse	Crevasse	Crevasse	206	8.4	86	1.6
	Full (9.3 kg)	206	1.7	17	0.7	206	1.4	6	1.3
		Peak moment	2.0 (231 ms)	33 (306 ms)	1.5 (306 ms)	Peak moment	1.7 (231 ms)	36 (231 ms)	2.4 (241 ms)
		306	0.6	33	1.5	306	0.8	31	2.1

5.2. Safe spacing and suggestions to prevent the failure of adjacent storage tanks

Once a detonation accident occurs in the storage tank, it will cause serious impact and huge property loss to the adjacent storage tank in the tank area. In order to ensure that the adjacent storage tank is not damaged, the initial energy of the explosive fragments should be determined, the critical speed of the explosive fragments of the detonation tank and the stress distribution of the adjacent storage tank are shown in Fig. 17. Let the maximum energy fragment initial velocity be V_n, After the fragments experiences air resistance and gravity, the velocity of flying near the tank is V_n', Now the maximum bonding unit node stress at the tank wall is if satisfied $\sigma^{eff} < \sigma_{fr}$, the maximum initial energy fragmentation velocity V_n shall meet the maximum fragmentation velocity of the adjacent tank; otherwise, V_n is reduced by 0.1 to V_{n+1}, V_{n+1} is applied to the explosive fragments, and the above process is repeated until the discriminant conditions are met. The measured initial velocity of the maximum energy fragment is recorded as shown in Table 9, and the stress cloud diagram of the fragment hitting the adjacent tank is shown in Fig. 17.

As can be seen from the data in Fig. 17 and Table 9, after adjusting the maximum energy fragments of the tank, the explosion velocity of the tank fragments between 5.0 m/s~5.8 m/s, and the impact near the tank, the stress near the tank yield strength below 235 MPa, indicating that the adjacent tank has been able to work safely.
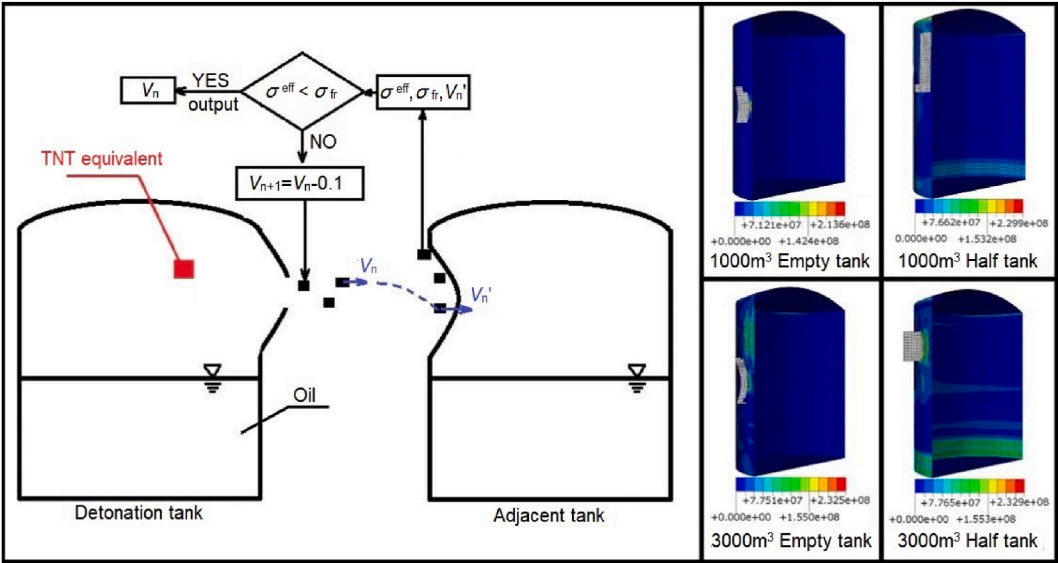
Fig. 17. Calculation process of critical velocity of fragments and stress nephogram of adjacent storage tank (Pa).

Table 9
Maximum energy fragment velocity and adjacent tank stress.

Storage tanks volume/m³	Liquid level	Fragment average Velocity/(m/s)	Maximum stress of adjacent tank/MPa
1000	Empty	5.8	213.6
	Half	5.3	229.9
3000	Empty	5.5	232.5
	Half	5.0	232.9

In order to further determine the spacing between tanks that do not cause the adjacent tanks, the tank spacing between different volume tanks was adjusted from 0.75D (0.6D) to 1.75D (1.6D) according to the requirements of document [34], and the velocity was calculated to Table 10.

As can be seen from Table 10, for the adjacent tank, when the tank spacing is 0.75D (0.6D), the fragment speed at the empty tank level decreases by about 27%, and the fragment speed at the half-tank level decreases by about 49%. It can be seen that the fragment speed of the half tank decreases more, but the maximum energy fragment speed still exceeds the critical speed to ensure the safe operation of the adjacent tank, and the adjacent tank still can not work safely. Therefore, we can control the operation of the tank at high liquid levels, or adjust the spacing to be less than the fragments speed of 5.0 m/s, to ensure the safe operation of the adjacent tank.

Table 10
Safety distance between detonation tank and adjacent tank.

Liquid level	Storage tanks volume	Tank spacing	Fragment average velocity/(m/s)	Difference	Adjacent working state
Empty	≤1000 m [3]	0.75D	83.0	−26.1%	×
		1.75D	61.3	−90.5%	×
		Safe spacing	5.8		✓
	≥3000 m [3]	0.6D	61.1	−28.5%	×
		1.6D	43.7	−87.4%	×
		Safe spacing	5.5		✓
Half	≤1000 m [3]	0.75D	96.0	−47.4%	×
		1.75D	50.5	−89.5%	×
		Safe spacing	5.3		✓
	≥3000 m [3]	0.6D	67.3	−51.6%	×
		1.6D	32.6	−84.7%	×
		Safe spacing	5.0		✓
Full	≤1000 m [3]	0.75D	–	–	✓
	≥3000 m [3]	0.6D	–	–	✓

5.3. Limitations and perspectives

This paper is based on the TNT-equivalent method to analyze the tank damage and adjacent tank response in the full-time domain process of bursting, the purpose is to analyze the distribution law of overpressure on the tank wall and explore the effect of debris flyaway on adjacent tanks, compared to the CESE IBM FSI solver combined with the appropriate chemical kinetics method, the values have errors at the closer position from the bursting center, in this paper the values are consistent between the 1000 m^{3}and 3000 m^3 volume tanks, for different locations within the tank, the overpressure values between the different locations of the size of the law is consistent. The author's next step will be the use of LS-DYNA in the CESE IBM FSI solver, combined with a simplified chemical kinetic model for accurate analysis of the combustible gas explosion inside the tank.

6. Conclusion

(i) This paper considers the multiphase coupling effect of liquid-tank-air, establishes the finite element model of the process in the tank process, and analyzes the whole time domain process under the different conditions of gas detonation in the tank by constructing the discrimination conditions for brittle fracture and failure of the storage tank materials, reproduces the structural response of the generation of explosive fragments and the failure of the tank explosion and adjacent tank in the whole time domain.

(ii) Empty tank and half tank produce fragments and explosion shock wave overpressure after detonation, directly opposite the explosion center (C_1 Point) is the first to explode, peak pressure; top wall junction (E_1 Point) where peak pressure is sublarge due to reflection enhancement effect; under full tank condition, the tank produces cracks but no fragments. During the entire detonation process, although the stress of the adjacent storage tank did not reach the yield strength of the material, the impact of the fragments has caused the crevasse of the adjacent tank, the empty tank and half tank completely lost the working capacity, and the full tank could still work.

(iii) As the liquid level increases, the shock wave overpressure of the detonation tank and adjacent tank decreases, resulting in stress and deformation, and the type and number of fragments. However, because the empty tank is broken before the pressure peaks, the pressure, stress and deformation are smaller than that of the half tank. With the increase of the tank volume, the shock wave overpressure and stress increase, the strain rate of the storage tank becomes larger, the tank is more prone to brittle failure, and the types and number of fragments formed increase. No fragments can be detonated in the full tank; for the empty tank and half tank state, you can increase the height of the liquid level or adjust the spacing until the maximum energy fragment speed is below 5.0 m/s to ensure the safe operation of the adjacent storage tank.

Data availability statement

Data related to the author's research are not deposited in public repositories, because the data included in article/supp. material/ referenced in article.

CRediT authorship contribution statement

Yuqi Ding: Methodology, Funding acquisition, Formal analysis, Data curation, Conceptualization. **Baishuai Li:** Validation, Software, Resources, Project administration. **Ye Lu:** Validation, Software, Resources, Project administration. **Ming Yang:** Visualization, Validation, Supervision, Software, Resources, Project administration. **Jiahe Zhang:** Writing – review & editing, Writing – original draft, Visualization, Funding acquisition, Formal analysis. **Qiaozhen Li:** Writing – review & editing, Writing – original draft, Visualization, Validation. **Kai Liu:** Writing – review & editing, Writing – original draft, Visualization, Validation.

Declaration of competing interest

The authors declare that they have no known competing financial interests or personal relationships that could have appeared to influence the work reported in this paper.

Acknowledgments

References

[1] D. Xu, Discussion on fire safety and fire rescue preparations in petrochemical enterprises, Fire Proc. Today. 1 (2022) 25–27.

[2] D.M. Yang, Response analysis of oil storage tank under explode disturbance, J. Wuhan Univ. Sci. Technol. (2020).

[3] M.S. Bi, Q.J. Ren, W. Sha, Etc. Key problems of storage safety of flammable liquefied gases under thermal invasion, J. Changzhou. Univ. Nat. Sci. Ed. 32 (4) (2020) 1–9.

[4] S.M. Wang, D.J. Wu, H. Guo, etc. Effects of concentration, temperature, ignition energy and relative humidity on the overpressure transients of fuel-air explosion in a medium-scale fuel tank, Fuel 259 (2020) 1–8.

[5] G. Chamberlain, E. Oran, A. Pekalski, Detonations in industrial vapour cloud explosions, J. Loss Prev. Process Ind. 62 (2019) 103918.

[6] L.Y. Cheng, C. Ji, M.S. Zhong, etc. Full-scale experimental investigation on the shock-wave characteristics of high-pressure natural gas pipeline physical explosions, Int. J. Hydrogen Energy. 44 (36) (2019) 20587–20597.

[7] Y. Lu, Y.Q. Ding, Z.T. Chen, Internal explosion load computation and structural response of storage tank based on heat-fluid-solid coupling, J. Failure Anal. and Prev. 21 (5) (2021) 1795–1807.

[8] K. Wang, T.T. Shi, Y.R. He, etc. Case analysis and CFD numerical study on gas explosion and damage processing caused by aging urban subsurface pipeline failures, Eng. Failure Anal. 97 (2019) 201–219.

[9] S. Høiset, B.H. Hjertager, T. Solberg, K.A. Malo, Flixborough revisited-an explosion simulation approach, J. Hazard. Mater. A77 (2000) 1–9.

[10] C.A. Pang, Z. Wang, Numerical simulation and dynamic response analysis of explosion in vertical cylindrical steel tank, BLASTING 32 (2) (2015) 54–58.

[11] Y.X. Cai, X.S. Jiang, S.M. Wang, etc. Experimental study on oil and gas explosion in simulated vertical dome roof oil tank, Explos. Shock Waves. 9 (2022) 1–19.

[12] H. Rokhy, H. Soury, Fluid structure interaction with a finite rate chemistry model for simulation of gaseous detonation metal-forming, Int. J. Hydrogen Energy. 44 (2019), 23289 e23302.

[13] H. Rokhy, H. Soury, Investigation of the confinement effects on the blast wave propagated from gas mixture detonation utilizing the CESE method with finite rate chemistry model, Combust. Sci. Technol. 194 (2021) 3003–3020.

[14] H. Rokhy, T.M. Mostofi, Tracking the explosion characteristics of the hydrogen-air mixture near a concrete barrier wall using CESE IBM FSI solver in LS-DYNA incorporating the reduced chemical kinetic model, Int. J. Imp. Eng. 172 (2023) 104401.

[15] T.M. Mostofi, H. Babaei, Plastic deformation of polymeric-coated aluminum plates subjected to gas mixture detonation loading : Part I : experimental studies, J. Solid and Fluid Mech. 9 (2019) 71–83.

[16] Y. Du, L. Ma, J.Y. Zheng, F. Zhang, A.D. Zhang, Numerical prediction on dynamic fracture of tubes subjected to internal gaseous detonation, Eng. Failure Anal. (2016).

[17] W.H. Wang, Study on Impact Assessment and Injury Prevention of Explosive Fragments in Chemical Industry Park, Univ .Pet., Beijing: China, 2017.

[18] U. Hauptmanns, A procedure for analyzing the flight of missiles from explosions of cylindrical vessels, J. Loss Prev. Process Ind. 14 (2001) 395–402.

[19] U. Nyström, K. Gylltoft, Numerical studies of the combined effects of blast and fragment loading, Int. J. Imp. Eng. 36 (2009) 995–1005.

[20] R. Feng, Z.X. Zhang, Q. Duan, etc. Study on fragments impact and protective measures of atmospheric vertical oil and gas storage tank, Pressure vessel 35 (4) (2018) 59–66.

[21] Z.L. Wang, Y. Jiang, Scenario deduction of domino effect in a tank farm fire, J. Fire Sci. 30 (2021) 54–61.

[22] S.Y. Chen, Numerical simulation of dynamic response characteristics of explosive fragments impacting on tank, Nanchang: J. Nanchang Univ. (2018).

[23] G.H. Chen, K. Hu, C.L. Zhou, etc. Simulation experiment of small size tank impacted by tip fragments, Explos. Shock Waves. 38 (2018) 1295–1302.

[24] S. Qi Study, On dynamic response and vulnerability of storage tank under the influence of explosive fragments, J. South China Univ. Technol. (2017).

[25] M. Djelosevic, G. Tepic, Identification of fragmentation mechanism and risk analysis due to explosion of cylindrical tank, J. Hazard. Mater. 362 (2019) 17–35.

[26] L. Ma, Y. Hu, J.Y. Zheng, G.D. Deng, Y.J. Chen, Failure analysis for cylindrical explosion containment vessels, Eng. Failure Anal. 17 (2010) 1221–1229.

[27] D.M. Yu, C.G. Feng, Destructive effect of explosion and damage zoning, China Saf. Sci. J. 5 (S1) (1995) 13–16.

[28] X.M. Qian, Y.B. Xu, Z.Y. Liu, Study on the harmfulness of BLEVE fragment ejection from spherical tank, Chin. J. High Pressure Phys. 23 (5) (2009) 389–394.

[29] X.M. Qian, Y.B. Xu, Z.Y. Liu, Monte-Carlo analysis of BLEVE fragment ejection from spherical tank, Chin. J. Chem. Eng. 60 (4) (2009) 1057–1061.

[30] Y.Q. Ding, Y. Lu, T. Lv, etc. Study on the influence of tank implosion radiation area based on numerical calculation method, Chem. Mach. 46 (2) (2019) 152–157 +181.

[31] L.G. Margolin, A generalized griffith criterion for crack propagation, Eng. Fract. Mech. (1984).

[32] J.K. Dienes, Comments on a generalized griffith criteria for crack propagation, Eng. Fract. Mech. 23 (3) (1986) 615–617.

[33] G.H. Chen, S. Qi, Numerical simulation of vertical tank impacted by explosive fragments, Sci. Technol. Work Saf. China. 12 (9) (2016) 115–119.

[34] GB50016-2014,《Fire Protection Code for Building Design》2018 Local Revision, 2018.